Application of the linear sampling method to retrieve cracks with impedance boundary conditions

Fahmi Ben Hassen, Yosra Boukari, Houssem Haddar

INRIA

INSTITUT NATIONAL DE RECHERCHE EN INFORMATIQUE ET EN AUTOMATIQUE

Application of the linear sampling method to retrieve cracks with impedance boundary conditions

Fahmi BEN HASSEN — Yosra BOUKARI — Houssem HADDAR

N° 7478

December 2010

Thème NUM

Rapport de recherche

ISSN 0249-6399 ISRN INRIA/RR--7478--FR+ENG

INSTITUT NATIONAL
DE RECHERCHE
EN INFORMATIQUE
ET EN AUTOMATIQUE

INRIA

centre de recherche
SACLAY - ÎLE-DE-FRANCE

Application of the linear sampling method to retrieve cracks with impedance boundary conditions

Fahmi BEN HASSEN* , Yosra BOUKARI*† , Houssem HADDAR†

Thème NUM — Systèmes numériques
Équipe-Projet DeFI

Rapport de recherche n° 7478 — December 2010 — 23 pages

Abstract: We use the Linear Sampling Method (LSM) to detect a crack with impedance boundary conditions. This paper extends the work of Cakoni and Colton [1] that uses the LSM to reconstruct a crack with mixed boundary conditions from measurements of the far field patterns associated with different incident plane waves. The performance of our method is illustrated through some numerical examples.

Key-words: Inverse scattering problems in electromagnetism and acoustics, detection of cracks, impedance boundary conditions, linear sampling method

* LAMSIN, Ecole Nationale D'ingénieurs de Tunis
† INRIA Saclay Ile de France / CMAP Ecole Polytechnique, Route de Saclay, 91128 Palaiseau, Cedex FRANCE

Centre de recherche INRIA Saclay – Île-de-France
Parc Orsay Université
4, rue Jacques Monod, 91893 ORSAY Cedex
Téléphone : +33 1 72 92 59 00

Application of the linear sampling method to retrieve cracks with impedance boundary conditions

Résumé : Nous utilisons dans ce travail la Linear Sampling Method pour reconstruire une fissure impédante dans le vide. Ce papier est une extension du travail de Cakoni et Colton [1] qui applique la Linear Sampling Method pour reconstruire une fissure avec une condition mixte et ceci en utilisant plusieurs mesures de champs lointains associés à différentes ondes incidentes planes. Nous donnons dans ce travail une validation théorique et numérique de notre méthode.

Mots-clés : Problème inverse en électromagnétisme, méthode d'échantillonnage, condition d'impédance, détection de fissure

1 Introduction

We are concerned in this work by the inverse scattering problem from a crack with an impedance boundary condition. More precisely we shall investigate the application of the Linear Sampling Method (LSM) to retrieve the geometry of the crack from multi-static far field data at a given frequency. As compared to previous works on this type of problem and methods [1, 4, 8], the originality of the present one relies on considering the case of the impedance boundary conditions on both sides of the crack. This induces more technical difficulties in the justification of the method and also on the numerical side. For instance the algorithm proposed in [1] does not work if one of the impedance values is not infinite. The main difficulty relies on the choice of the orientation of the probing " small " crack. Based on the theoretical justification of LSM we propose a minimization procedure that enforces the correct choice of this orientation. Prior to considering the inverse problem, we propose a study of the forward problem using an integral equation approach. This part is then used in designing a numerical method to solve this problem. It is used for instance, to generate the synthetic data needed for the inverse scheme. The theoretical developments of this first part are inspired by [1]. We also quote the work of [9] for the study of the direct problem using an integral equation approach in Hölder spaces and the work of [10] for the study of the inverse problem using a different sampling method. The extension of the current work to the factorization method [7] and to the reciprocity gap sampling method [2] is under preparation.

The report is organized as follows. In section 2, the direct problem is introduced along with a study of the uniqueness and existence of the solution using an integral equation method. The validation of the numerical implementation of this problem is then presented by comparing the results to those given by a volumetric method (using FreeFem++ [6]). In section 3, we introduce the inverse problem and we describe our formulation of the LSM along with the mathematical justifications. Lastly, we propose and test different sampling schemes associated with section 3, for different shapes of the cracks and different values of the impedances.

2 The direct scattering problem for a crack with impedance boundary conditions

Let $\sigma \subset \mathbf{R}^m$, $m = 2, 3$, be a smooth nonintersecting open arc. For further considerations, we assume that σ can be extended to an arbitrary smooth, closed curve $\partial\Omega$ enclosing a bounded domain Ω in $\mathbf{R}^m$. The normal vector ν on σ coincides with the outward normal vector to $\partial\Omega$, with simply connected complement.
Impedance type boundary conditions on σ lead to the following problem

$$\begin{cases} \Delta u + k^2 u = 0 & \text{in } \mathbf{R}^m \setminus \overline{\sigma} \\ \partial_\nu u_\pm \pm \lambda^\pm u_\pm = 0 & \text{on } \sigma \end{cases} \tag{1}$$

where the wave number k is positive and $\lambda_\pm \in L^\infty(\sigma)$ are the given (complex-valued) impedance functions with non-negative imaginary part and $\lambda^+ + \lambda^- \neq 0$. Notice that $u_\pm(x) = \lim_{h\to 0^+} u(x \pm h\nu)$ and $\partial_\nu u_\pm = \lim_{h\to 0^+} \nu \cdot \nabla u(x \pm h\nu)$ for $x \in \sigma$.
The total field $u = u^i + u^s$ is decomposed into the given incident plane wave $u^i(x, d) = e^{ikd\cdot x}$ with unitary direction d and the unknown scattered field u^s which is required to satisfy the Sommerfeld radiation condition

$$\lim_{r=|x|\to+\infty} r^{\frac{m-1}{2}} (\partial_r u^s - iku^s) = 0, \tag{2}$$

uniformly in all directions $\hat{x} = \frac{x}{|x|}$.
In order to formulate the scattering problem more precisely we need to define the trace spaces on σ. If $H^1_{loc}(\mathbf{R}^m \setminus \overline{\sigma})$, $H^{1/2}(\partial\Omega)$ and $H^{-1/2}(\partial\Omega)$ denote the usual Sobolev spaces we define the following spaces (see [11]) :

$$H^{1/2}(\sigma) = \left\{ u_{|\sigma} : u \in H^{1/2}(\partial\Omega) \right\}$$
$$\tilde{H}^{1/2}(\sigma) = \left\{ u \in H^{1/2}(\sigma) : supp(u) \subset \bar{\sigma} \right\}.$$

Now we denote by $H^{-1/2}(\sigma)$ and $\tilde{H}^{-1/2}(\sigma)$ the dual spaces of $\tilde{H}^{1/2}(\sigma)$ and $H^{1/2}(\sigma)$ respectively. Using the notation

$$g^{\pm} = -(\partial_\nu u^i \pm \lambda^{\pm} u^i) \tag{3}$$

the problem (1)-(2) is a special case of the

Impedance crack problem (ICP) : Given $g^{\pm} \in H^{-1/2}(\partial\Omega)$ and $(\lambda^{\pm}) \in L^\infty(\sigma)$ with $Im(\lambda^{\pm}) \geq 0$ and $\lambda^+ \neq -\lambda^-$, find $u^s \in H^1_{loc}(\mathbf{R}^m \setminus \overline{\sigma})$ satisfying the Sommerfeld radiation condition (2) and

$$\Delta u^s + k^2 u^s = 0 \quad \text{in } \mathbf{R}^m \setminus \overline{\sigma} \tag{4}$$

$$\partial_\nu u^s_{\pm} \pm \lambda^{\pm} u^s_{\pm} = g^{\pm} \qquad \text{on } \sigma. \tag{5}$$

The aim of this section is to prove the existence of the solution of the (ICP) problem, since the following uniqueness result can be found in [9] and [4]

Theorem 1 *The (ICP) problem has at most one solution.*

To prove the existence of the solution of the (ICP), we use a boundary integral equations approach (see [4] for a sound soft crack and a sound hard crack, [1] for a partially coated crack and [9] for a 2D impedance crack when $\lambda^+ = \lambda^-$ is Hölder continuous).
We define $[u] := u_+ - u_-$ and $[\partial_\nu u] := \partial_\nu u_+ - \partial_\nu u_-$, the jump of u and $\partial_\nu u$ respectively, across the crack σ.

Lemma 1 *Further assume that $(\lambda^{\pm})^{-1} \in L^\infty(\sigma)$. The scattered field u^s is solution of the (ICP) if and only if the vector $([u], [\partial_\nu u])^T$ solves the system of integral equations*

$$A_\sigma \begin{pmatrix} [u] \\ \\ [\partial_\nu u] \end{pmatrix} = \begin{pmatrix} -(\lambda^+ + \lambda^-)\partial_\nu u^i \\ \\ -(\lambda^+ + \lambda^-)u^i \end{pmatrix} \tag{6}$$

where the matrix operator $A_\sigma : \tilde{H}^{1/2}(\sigma) \times \tilde{H}^{-1/2}(\sigma) \to H^{-1/2}(\sigma) \times H^{-1/2}(\sigma)$ is given by

$$A_\sigma := \begin{pmatrix} \lambda^+\lambda^- I + (\lambda^+ + \lambda^-)T_\sigma & -\dfrac{1}{2}(\lambda^+ - \lambda^-)I - (\lambda^+ + \lambda^-)K'_\sigma \\ \\ \dfrac{1}{2}(\lambda^+ - \lambda^-)I + (\lambda^+ + \lambda^-)K_\sigma & I - (\lambda^+ + \lambda^-)S_\sigma \end{pmatrix} \tag{7}$$

Proof
If u^s is a solution of the (ICP) then $[u^s] \in \tilde{H}^{1/2}(\sigma)$ and $[\partial_\nu u^s] \in \tilde{H}^{-1/2}(\sigma)$ (see Lemma 2.2 in [1]). Using the Green representation formula, the following relation holds for $z \in \mathbf{R}^m \setminus \overline{\sigma}$ (see theorem 2.24 in [4])

$$u^s(z,d) = \int_\sigma \left([u(y,d)] \frac{\partial \Phi(z,y)}{\partial \nu(y)} - \left[\frac{\partial u(y,d)}{\partial \nu(y)} \right] \Phi(z,y) \right) ds(y), \tag{8}$$

where Φ is the fundamental solution to the Helmholtz equation defined by

$$\Phi(x,y) := \begin{cases} \dfrac{1}{4\pi} \dfrac{e^{i\kappa|x-y|}}{|x-y|} & m = 3 \\ \dfrac{i}{4} H_0^{(1)}(\kappa|x-y|) & m = 2 \end{cases}$$

with $x \neq y$ and $H_0^{(1)}$ being the Hankel function of the first kind of order zero. Next by making use of the jump relations of the single and double layer potentials across $\partial\Omega$ (see [11]), we obtain from (8)

$$u^s_{\pm} = K_\sigma[u] - S_\sigma[\partial_\nu u] \pm \frac{1}{2}[u] \tag{9}$$

$$\partial_\nu u^s_{\pm} = T_\sigma[u] - K'_\sigma[\partial_\nu u] \pm \frac{1}{2}[\partial_\nu u] \tag{10}$$

where $S_{\partial\Omega}, K_{\partial\Omega}, K'_{\partial\Omega}, T_{\partial\Omega}$ are the boundary integral operators

$$\begin{array}{ll} S_{\partial\Omega} : H^{-1/2}(\partial\Omega) \to H^{1/2}(\partial\Omega) & K_{\partial\Omega} : H^{1/2}(\partial\Omega) \to H^{1/2}(\partial\Omega) \\ K'_{\partial\Omega} : H^{-1/2}(\partial\Omega) \to H^{-1/2}(\partial\Omega) & T_{\partial\Omega} : H^{1/2}(\partial\Omega) \to H^{-1/2}(\partial\Omega) \end{array}$$

defined by

$$\begin{array}{ll} S_{\partial\Omega}\psi(x) := \displaystyle\int_{\partial\Omega} \psi(y)\Phi(x,y)ds(y), & K_{\partial\Omega}\varphi(x) := \displaystyle\int_{\partial\Omega} \varphi(y)\frac{\partial\Phi(x,y)}{\partial\nu(y)}ds(y), \\ K'_{\partial\Omega}\psi(x) := \displaystyle\int_{\partial\Omega} \psi(y)\frac{\partial\Phi(x,y)}{\partial\nu(x)}ds(y), & T_{\partial\Omega}\varphi(x) := \displaystyle\frac{\partial}{\partial\nu(x)}\int_{\partial\Omega} \varphi(y)\frac{\partial\Phi(x,y)}{\partial\nu(y)}ds(y) \end{array}$$

and $S_\sigma, K_\sigma, K'_\sigma, T_\sigma$ are the corresponding operators defined on σ. These restricted operators have the following mapping properties (see [11])

$$\begin{array}{ll} S_\sigma : H^{-1/2}(\sigma) \to H^{1/2}(\sigma) & K_\sigma : H^{1/2}(\sigma) \to H^{1/2}(\sigma) \\ K'_\sigma : H^{-1/2}(\sigma) \to H^{-1/2}(\sigma) & T_\sigma : H^{1/2}(\sigma) \to H^{-1/2}(\sigma). \end{array}$$

Moreover, from the boundary conditions (5) and (3), we have

$$\begin{aligned} &[\partial_\nu u] + \lambda^+ u^s_+ + \lambda^- u^s_- = -(\lambda^+ + \lambda^-)u^i, \\ &\lambda^+\lambda^-[u] + \lambda^- \partial_\nu u^s_+ + \lambda^+ \partial_\nu u^s_- = -(\lambda^+ + \lambda^-)\partial_\nu u^i. \end{aligned} \tag{11}$$

Finally, by combining the relations (9), (10) and (11), we show that $([u], [\partial_\nu u])^T$ solves the system of equations (6).

Conversely, assume that $([u], [\partial_\nu u])^T$ satisfies (6)-(7), so

$$\lambda^- \left(T_\sigma[u] - K'_\sigma[\partial_\nu u] + \frac{[\partial_\nu u]}{2} \right) + \lambda^+ \left(T_\sigma[u] - K'_\sigma[\partial_\nu u] - \frac{[\partial_\nu u]}{2} \right) + \lambda^+\lambda^-[u] = -(\lambda^+ + \lambda^-)\partial_\nu u^i \tag{12}$$

and

$$\lambda^+ \left(K_\sigma[u] - S_\sigma[\partial_\nu u] + \frac{[u]}{2} \right) + \lambda^- \left(K_\sigma[u] - S_\sigma[\partial_\nu u] - \frac{[u]}{2} \right) + [\partial_\nu u] = -(\lambda^+ + \lambda^-)u^i \tag{13}$$

The potential u^s, defined by (8), belongs to $H^1_{loc}(\mathbf{R}^m \setminus \overline{\sigma})$ and satisfies the Helmholtz equation in $\mathbf{R}^m \setminus \sigma$ and the Sömmerfeld radiation condition. It remains to show that u^s satisfies the boundary condition (5). To this end, we first inject (10) in (12) and (9) in (13). We obtain

$$\lambda^- \partial_\nu u^s_+ + \lambda^+ \partial_\nu u^s_- + \lambda^+\lambda^- [u] = -(\lambda^+ + \lambda^-)\partial_\nu u^i \tag{14}$$

$$\lambda^+ u^s_+ + \lambda^- u^s_- + [\partial_\nu u] = -(\lambda^+ + \lambda^-)u^i \tag{15}$$

Multiplying (15) by $\lambda^\pm$ and adding the results to (14), we show that

$$\partial_\nu u^s_\pm - \lambda^\pm u^s_\pm = -(\partial_\nu u^i \pm \lambda^\pm u^i) \quad \text{on } \sigma.$$

Therefore, the field u^s given by (8) is a solution of the (ICP). □

Lemma 2 *The operator A_σ given by (7) has a trivial kernel.*

Proof.
Let $\zeta = (\alpha, \beta)^T \in \tilde{H}^{1/2}(\sigma) \times \tilde{H}^{-1/2}(\sigma)$ satisfying $A_\sigma\zeta = 0$. Define the potential

$$v = \int_\sigma \frac{\partial\Phi(x,y)}{\partial n(y)}\alpha(y)ds(y) - \int_\sigma \Phi(x,y)\beta(y)ds(y); \quad x \in \mathbf{R}^m \setminus \overline{\sigma}.$$

This potential belongs to $H^1_{loc}(\mathbf{R}^m \setminus \overline{\sigma})$ and satisfies the Helmholtz equation in $\mathbf{R}^m \setminus \sigma$ and the Sommerfeld radiation condition. Moreover, using the jump relations of the single and double layer potentials across σ, we get

$$v_\pm = K_\sigma(\alpha) - S_\sigma(\beta) \pm \frac{\alpha}{2}$$
$$\partial_\nu v_\pm = T_\sigma(\alpha) - K'_\sigma(\beta) \pm \frac{\beta}{2}$$

Hence,

$$[v] = \alpha \text{ and } [\partial_\nu v] = \beta. \tag{16}$$

Therefore, as in the proof of Lemma 1, we show that $v \in H^1_{loc}(\mathbf{R}^2 \setminus \bar{\sigma})$ satisfies

$$\Delta v + k^2 v = 0 \quad \text{in } \mathbf{R}^2 \setminus \sigma,$$
$$\partial_\nu v_\pm - \lambda^\pm v_\pm = 0 \qquad \text{on } \sigma$$

and the Sömmerfeld radiation condition. Then, from the uniqueness of the solution of this system, we have $v = 0$ and we conclude, by (16), that $\alpha = \beta = 0$. □

Lemma 3 *The operator $A_\sigma : \tilde{H}^{1/2}(\sigma) \times \tilde{H}^{-1/2}(\sigma) \to H^{-1/2}(\sigma) \times H^{-1/2}(\sigma)$ given by (7) has a bounded inverse.*

Proof.
Let $\varphi \in H^{1/2}(\partial\Omega)$ and $\psi \in H^{-1/2}(\partial\Omega)$ be the extension by zero to $\partial\Omega$ of $[u] \in \tilde{H}^{1/2}(\sigma)$ and $[\partial_\nu u] \in \tilde{H}^{-1/2}(\sigma)$ respectively. We denote by T_0 the boundary integral operator corresponding to the Laplace operator, defined as $T_{\partial\Omega}$ by replacing the kernel $\Phi(x,y)$ by

$$\Phi_0(x,y) := \begin{cases} \dfrac{1}{4\pi}\dfrac{1}{|x-y|} & m = 3 \\ -\dfrac{1}{2\pi}\ln|x-y| & m = 2 \end{cases}$$

The operator $-T_0$ is coercive on $\partial\Omega$. Hence, we have for all $\varphi \in H^{1/2}(\partial\Omega)$

$$Re(\langle -T_0\varphi, \varphi\rangle_{H^{-1/2}(\partial\Omega), H^{1/2}(\partial\Omega)}) \geq \|\varphi\|_{H^{1/2}(\partial\Omega)}.$$

Then

$$Re(\langle -T_0[u], [u]\rangle_{H^{-1/2}(\sigma), \tilde{H}^{1/2}(\sigma)}) \geq \|[u]\|_{\tilde{H}^{1/2}(\sigma)},$$

which leads to the coercivity of the operator $-T_0$ on σ whence the operator

$$A_{0,\sigma} = \begin{pmatrix} (\lambda^+ + \lambda^-)T_0 & -\frac{1}{2}(\lambda^+ + \lambda^-)I \\ 0 & I \end{pmatrix}$$

is invertible. Consider now the operator

$$A_c = \begin{pmatrix} \lambda^+\lambda^- I + (\lambda^+ + \lambda^-)T_c & -(\lambda^+ + \lambda^-)K'_{\partial\Omega} \\ \dfrac{\lambda^+ - \lambda^-}{2} I + (\lambda^+ + \lambda^-)K_{\partial\Omega} & -(\lambda^+ + \lambda^-)S_{\partial\Omega}. \end{pmatrix}$$

The operator $T_c := T_{\partial\Omega} - T_0$ is compact since it has a continuous kernal.
Since the injection from $H^{\frac{1}{2}}(\partial\Omega)$ to $H^{-\frac{1}{2}}(\partial\Omega)$ is compact and $\lambda^\pm \in L^\infty(\partial\Omega)$, the operators $(\lambda^+ - \lambda^-)I$ and $\lambda^+\lambda^- I$ are also compact from $H^{\frac{1}{2}}(\partial\Omega)$ to $H^{-\frac{1}{2}}(\partial\Omega)$.
In the other hand, $K'_{\partial\Omega}$ is a compact operator from $H^{-\frac{1}{2}}(\partial\Omega)$ to $H^{-\frac{1}{2}}(\partial\Omega)$. The operator $S_{\partial\Omega}$ is continuous from $H^{-\frac{1}{2}}(\partial\Omega)$ to $H^{\frac{1}{2}}(\partial\Omega)$. Thus $(\lambda^+ + \lambda^-)S_{\partial\Omega}$ is compact from $H^{-\frac{1}{2}}(\partial\Omega)$ to $H^{-\frac{1}{2}}(\partial\Omega)$. The operator $K_{\partial\Omega}$ is continuous from $H^{\frac{1}{2}}(\partial\Omega)$ to $H^{\frac{1}{2}}(\partial\Omega)$, which implies that $(\lambda^+ +$

$\lambda^-)K_{\partial\Omega}$ is compact from $H^{\frac{1}{2}}(\partial\Omega)$ to $H^{-\frac{1}{2}}(\partial\Omega)$. We conclude that $A_c : \tilde{H}^{1/2}(\partial\Omega) \times \tilde{H}^{-1/2}(\partial\Omega) \to H^{-1/2}(\partial\Omega) \times H^{-1/2}(\partial\Omega)$ is a compact operator. Thus the restriction of A_c to $\tilde{H}^{1/2}(\sigma) \times \tilde{H}^{-1/2}(\sigma)$ denoted by $A_{c,\sigma}$ is also compact.
Finally $A_\sigma = A_{0,\sigma} + A_{c,\sigma}$ is Fredholm with index zero and since by Lemma 2 A_σ is injective we conclude that it has a bounded inverse. □
As a consequence of these lemmas, we have the following result

Theorem 2 *The (ICP) problem has a unique solution given by*

$$u^s(z,d) = \int_\sigma \left([u(y,d)] \frac{\partial \Phi(z,y)}{\partial \nu(y)} - \left[\frac{\partial u(y,d)}{\partial \nu(y)} \right] \Phi(z,y) \right) ds(y), \quad z \in \mathbf{R}^m \setminus \overline{\sigma} \tag{17}$$

where, $([u], \partial_\nu u])^T$ *is the unique solution of the system of integral equations (6).*

2.1 Numerical solution of the (ICP) problem

Let $A_\sigma : \tilde{H}^{1/2}(\sigma) \times \tilde{H}^{-1/2}(\sigma) \to H^{-1/2}(\sigma) \times H^{-1/2}(\sigma)$ be the matrix operator given by (7). We use a Galerkin method to solve numerically the system of integral equations

$$A_\sigma \begin{pmatrix} \varphi \\ \psi \end{pmatrix} = \begin{pmatrix} f_1 \\ f_2 \end{pmatrix}. \tag{18}$$

We multiply the two equations in (18) by test functions α and $\beta \in \tilde{H}^{\frac{1}{2}}(\sigma)$ respectively and we integer over σ (in the sense of the duality pairing between $H^{-1/2}(\sigma)$ and $\tilde{H}^{\frac{1}{2}}(\sigma)$)

$$\int_\sigma \lambda^+\lambda^- \alpha\varphi + \int_\sigma C_1 \alpha T_\sigma \varphi - \int_\sigma C_2 \alpha\psi - \int_\sigma C_1 \alpha K'_\sigma \psi = \int_\sigma \alpha f_1 \tag{19}$$

$$\int_\sigma C_1 \beta\varphi + \int_\sigma C_2 \beta K_\sigma \varphi + \int_\sigma \lambda^+\lambda^- \beta\psi - \int_\sigma C_1 \beta S_\sigma \psi = \int_\sigma \beta f_2 \tag{20}$$

where we simplified the notations by denoting $C_1 = (\lambda^+ + \lambda^-)$, $C_2 = \frac{1}{2}(\lambda^+ - \lambda^-)$.
Then we discretize the space $H^{-1/2}(\sigma) \times \tilde{H}^{1/2}(\sigma)$ using finite elements $P_1 \times P_1$. To compute the integral involving the operator T_σ we use the following formula (see [5])

$$\begin{aligned} &\int_\sigma \alpha(x) \frac{\partial}{\partial \nu(x)} \int_\sigma \varphi(y) \frac{\partial \Phi(x,y)}{\partial \nu(y)} \, ds(y) \, ds(x) \\ &= \kappa^2 \int_\sigma \int_\sigma \Phi(x,y) \nu(x) \cdot \nu(y) \alpha(x) \varphi(y) \, ds(x) \, ds(y) \\ &- \int_\sigma \int_\sigma \Phi(x,y) (\nabla \alpha(x) \times \nu(x)) \cdot (\nabla \varphi(y) \times \nu(y)) \, ds(x) \, ds(y). \end{aligned}$$

We end the study of the direct problem by some numerical tests obtained by the scheme described above. To validate our algorithm, we use also FreeFem++ to solve (ICP) problem using FEM method. To this end, we discretize the disk of radius 10 times the wavelength by $P1$ elements. We compare the modulus of the far field pattern (see (21)), computed by the two methods (the scheme based on integral equations and that using FEM) for 100 observation points, different crack shapes and different incident plane waves $u^i(x) = \exp(ik(x_1 cos(\theta) + x_2 sin(\theta)))$ with angle θ. We keep the wave number constant $k = 2\pi$ for all the tests and we choose two different values of the impedances $\lambda^- = \lambda^+ = 5 + i$ and $\lambda^- = \lambda^+ = 1 + i$.
We recall that the solution of the (ICP) problem has the asymptotic behaviour of an outgoing spherical wave (see [3])

$$u^s(x,d) = r^{\frac{1-m}{2}} e^{ikr} u^\infty(\hat{x}, d) + O(r^{-\frac{m+1}{2}}), \tag{21}$$

where u^∞ is the far field pattern of the scattered wave, $x \in \mathbb{R}^m \setminus \overline{\sigma}$, $\hat{x} = x/|x|$ and $r = |x|$.

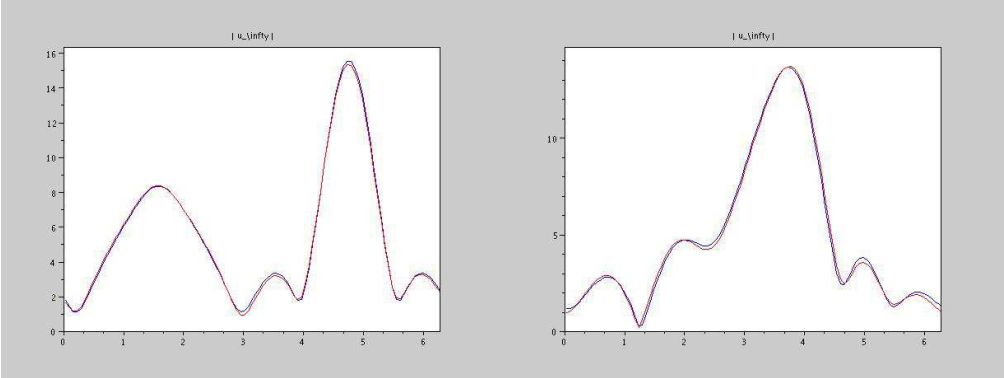

Figure 1: The modulus of u^∞ computed by Freefem++ (red) and by the integral equations method (blue) for $\lambda^- = \lambda^+ = 5 + i$. The angle of incidence $\theta = \pi/2$ (left) and $\theta = \pi/6$ (right). The crack is the segment $[-0.5,\ 0.5] \times \{0\}$.

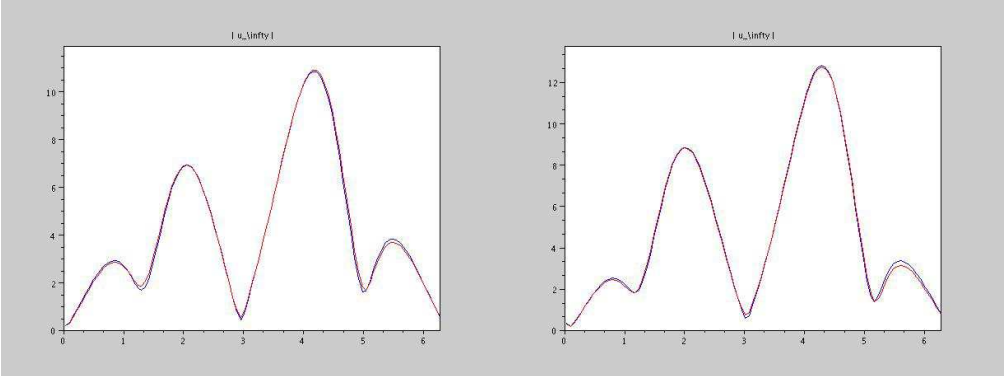

Figure 2: The modulus of u^∞ computed by Freefem++ (red) and by the integral equations method (blue) for $\lambda^- = \lambda^+ = 1 + i$. The angle of incidence $\theta = \pi/4$ (left) and $\theta = \pi/3$ (right). The crack is the segment $\{0\} \times [-0.5,\ 0.5]$.

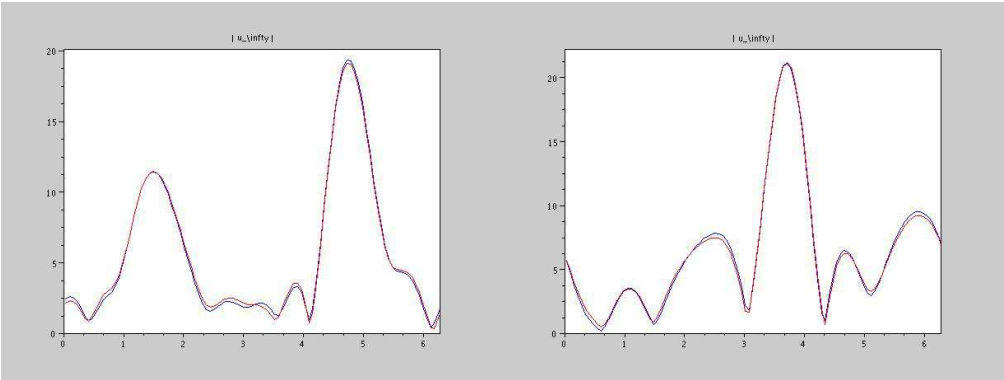

Figure 3: The modulus of u^∞ computed by Freefem++ (red) and by the integral equations method (blue) for $\lambda^- = \lambda^+ = 5 + i$. The angle of incidence $\theta = \pi/2$ (left) and $\theta = \pi/6$ (right). The crack is of shape L with peaks $(0, 1), (1, 1), (1, 0)$.

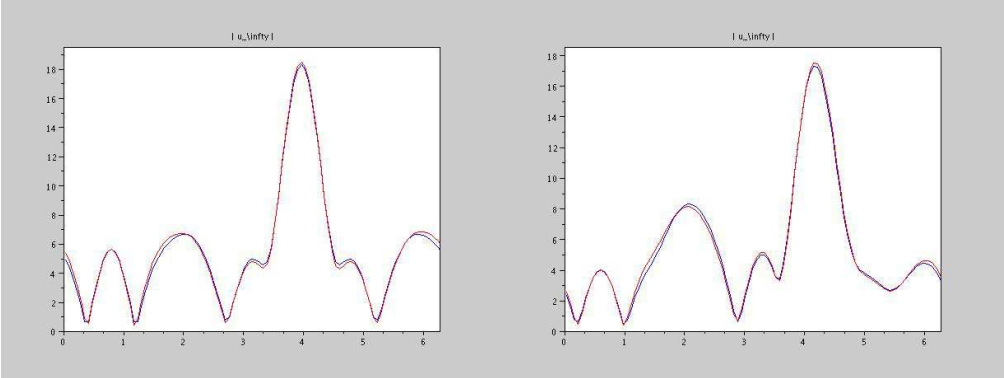

Figure 4: The modulus of u^∞ computed by Freefem++ (red) and by the integral equations method (blue) for $\lambda^- = \lambda^+ = 1 + i$, $\theta = \pi/4$ (left) and $\theta = \pi/3$ (right). The crack is is of shape L with peaks $(0, 1), (1, 1), (1, 0)$.

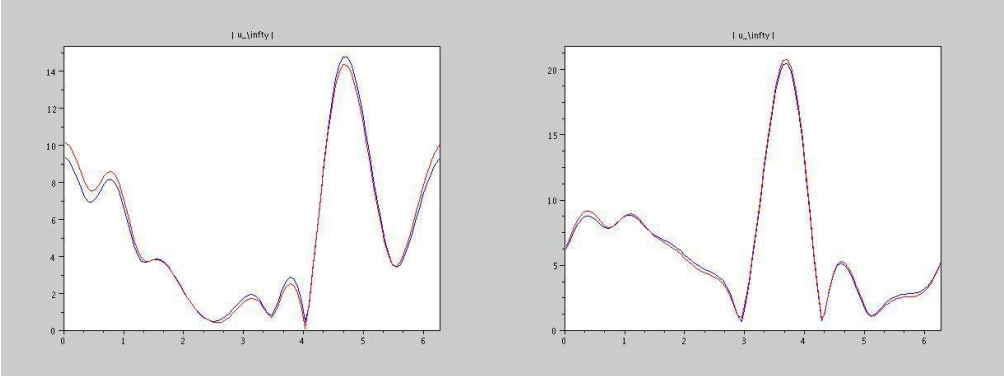

Figure 5: The modulus of u^∞ computed by Freefem++ (red) and by the integral equations method (blue) for $\lambda^- = \lambda^+ = 5 + i$, $\theta = \pi/2$ (left) and $\theta = \pi/6$ (right). The crack is an arc of the unit circle with an angle varying from 0 to 90 degrees.

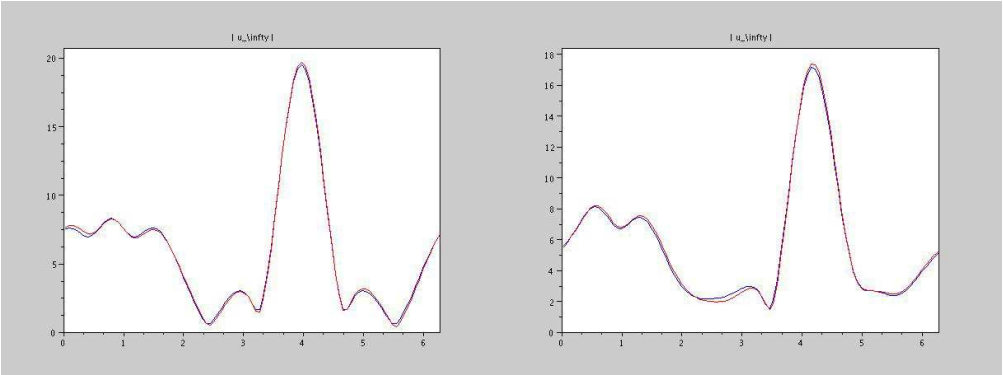

Figure 6: The modulus of u^∞ computed by Freefem++ (red) and by the integral equations method (blue) for $\lambda^- = \lambda^+ = 1 + i$, $\theta = \pi/4$ (left) and $\theta = \pi/3$ (right). The crack is an arc of the unit circle with an angle varying from 0 to 90 degrees.

We can clearly see that the results (compare Figure 1 to 6) obtained by the two methods are very close which validates our scheme. Note that the integral equation method is much faster than the finite element method since the size of the linear system is much smaller (even though, the matrix is not sparse).

3 The inverse problem

3.1 Settings and theoretical justification of the LSM

In this section, we adapt the LSM for scattering by a partially coated crack (see [1]) to the following inverse problem :

Inverse scattering by an Impedance Crack (IIC). *Given the far field pattern $u^\infty(\cdot,\cdot)$ on $\mathbf{S}^{m-1}\times\mathbf{S}^{m-1}$ of the solution to (ICP), reconstruct the crack σ.*

To solve the (IIC) by the LSM method, we first define the far field operator

$$\begin{array}{rccc} F: & L^2(\mathbf{S}^{m-1}) & \to & L^2(\mathbf{S}^{m-1}) \\ & g & \mapsto & \displaystyle\int_{\mathbf{S}^{m-1}} u^\infty(\cdot,y)g(y)ds(y) \end{array} \tag{22}$$

and consider the far field equation

$$F(g_L)(\hat{x}) = \Phi_L^\infty(\hat{x}) \qquad \text{for all} \quad \hat{x}\in\mathbf{S}^{m-1} \tag{23}$$

where $\Phi_L^\infty \in L^2(\mathbf{S}^{m-1})$ is given by

$$\Phi_L^\infty(\hat{x}) = \gamma\int_L \left(\alpha_L(y)\frac{\partial e^{-i\kappa\hat{x}\cdot y}}{\partial\nu(y)} + \beta_L(y)e^{-i\kappa\hat{x}\cdot y}\right)ds(y), \tag{24}$$

$$\text{with } \gamma = \begin{cases} \dfrac{e^{i\pi/4}}{\sqrt{8\pi\kappa}} & \text{in } 2D \\ \dfrac{1}{4\pi} & \text{in } 3D \end{cases} \tag{25}$$

Notice that Φ_L^∞ is the far field pattern of the potential Φ_L defined by

$$\Phi_L(x) := \int_L \left(\alpha_L(y)\frac{\partial\Phi(x,y)}{\partial\nu(y)} + \beta_L(y)\Phi(x,y)\right)ds(y) \tag{26}$$

with densities $\alpha_L \in \tilde{H}^{\frac{1}{2}}(L)$ and $\beta_L \in \tilde{H}^{-\frac{1}{2}}(L)$, for any smooth non intersecting open arc $L\in\mathbb{R}^{m-1}$. We will characterize the crack σ by the behaviour of an approximate solution g_L of the far field equation (23).

To prove the existence of an approximate solution of (23), we factorize the operator F as $F = B\mathcal{H}$ where $B : H^{-1/2}(\sigma)\times H^{-1/2}(\sigma) \to L^2(\mathbf{S}^{m-1})$ maps the boundary data (g^+, g^-) to the far field pattern of the solution of (ICP) and $\mathcal{H}$ is the trace operator defined by

$$\begin{array}{rccc} \mathcal{H}: & L^2(\mathbf{S}^{m-1}) & \to & H^{-1/2}(\sigma)\times H^{-1/2}(\sigma) \\ & g & \mapsto & ((\partial_\nu - \lambda^-)v_g, (\partial_\nu+\lambda^+)v_g) \end{array}$$

where v_g is the Herglotz wave function of kernal $g\in L^2(\mathbf{S}^{m-1})$,

$$v_g(x) := \int_{\mathbf{S}^{m-1}} e^{i\kappa x\cdot d}g(d)\,ds(d), \quad x\in\mathbb{R}^m. \tag{27}$$

We will show that the traces of the solution of the (ICP) on both sides of σ can be approximated by the appropriate traces of the Herglotz wave function v_g. We shall keep the same hypothesis on $\lambda^\pm$ as in section 2 and further assume that $(\lambda^+ + \lambda^-)(x) \neq 0$ for a.e $x\in\sigma$.

Lemma 4 *The operator $\mathcal{H}$ is injective and has a dense range.*

Proof. Let $g \in L^2(\mathbf{S}^{m-1})$ be an element of the kernal of $\mathcal{H}$. Then,

$$(\partial_\nu \pm \lambda^\pm) v_g = 0 \text{ on } \sigma.$$

Since by assumption $(\lambda^+ + \lambda^-) \neq 0$ then $v_g = 0$ and $\partial_\nu v_g = 0$ on $\sigma_0 \subset \sigma$. From the unique continuation principle it implies that $v_g = 0$ in $\mathbb{R}^m$ and therefore $g = 0$ which proves that $\mathcal{H}$ is one to one.
The main idea of the proof of the second part of the theorem is to show that $\mathcal{H}^*$, the adjoint operator of $\mathcal{H}$, is injective.
To this end, we determine first the expression of $\mathcal{H}^*$. Let $g \in L^2(\mathbf{S}^{m-1})$ and $\alpha, \beta \in \tilde{H}^{1/2}(\sigma)$, then $\mathcal{H}^* : \tilde{H}^{1/2}(\sigma) \times \tilde{H}^{1/2}(\sigma) \to L^2(\mathbf{S}^{m-1})$ satisfies

$$\langle \mathcal{H}(g), (\alpha, \beta) \rangle_{H^*, H} = \langle g, \mathcal{H}^*(\alpha, \beta) \rangle_{L^2(\mathbf{S}^{m-1}), L^2(\mathbf{S}^{m-1})}$$

where $H := \tilde{H}^{1/2}(\sigma) \times \tilde{H}^{1/2}(\sigma)$.
By changing the order of integration and using (27),

$$\langle \mathcal{H}(g), (\alpha, \beta) \rangle_{H^*, H}$$
$$= \int_{\mathbf{S}^{m-1}} g(d) \left[\int_\sigma \left(\alpha(y) \left(\frac{\partial}{\partial \nu(y)} - \lambda^- \right) + \beta(y) \left(\frac{\partial}{\partial \nu(y)} + \lambda^+ \right) \right) e^{-i\kappa d \cdot y} ds(y) \right] ds(d).$$

Therefore, for $d \in \mathbf{S}^{m-1}$, the operator $\mathcal{H}^*$ is given by

$$\mathcal{H}^*(\alpha, \beta)(d) = \int_\sigma \left(\alpha(y) \left(\frac{\partial}{\partial \nu(y)} - \lambda^- \right) e^{-i\kappa d \cdot y} + \beta(y) \left(\frac{\partial}{\partial \nu(y)} + \lambda^+ \right) e^{-i\kappa d \cdot y} \right) ds(y).$$

We observe that $\mathcal{H}^*$ is the far field pattern of the potential

$$\gamma^{-1} V(z) = \int_\sigma (\alpha(y) \left(\frac{\partial}{\partial \nu(y)} - \lambda^- \right) \Phi(z, y) + \beta(y) \left(\frac{\partial}{\partial \nu(y)} + \lambda^+ \right) \Phi(z, y)) ds(y),$$

for $z \in \mathbb{R}^m \setminus \bar{\sigma}$. This function is well defined in $\mathbb{R}^m \setminus \bar{\sigma}$ since α and β can be extended by zero to functions in $H^{1/2}(\sigma)$. Moreover, $V \in H^1_{loc}(\mathbb{R}^m \setminus \bar{\sigma})$ satisfies the Helmholtz equation and the sommerfeld radiation condition.
Therefore, if $\mathcal{H}^*(\alpha, \beta) = 0$, the far field pattern of V is zero and from Rellich's lemma and the unique continuation principle we conclude that $V = 0$ in $\mathbb{R}^m \setminus \bar{\sigma}$. Then, by the jump relations of the layer potentials, we have $[V] = \gamma(\alpha + \beta)$ and $[\partial_\nu V] = \gamma(\lambda^- \alpha - \lambda^+ \beta)$. This implies that

$$\alpha + \beta = 0 \quad \text{and} \quad \lambda^- \alpha - \lambda^+ \beta = 0.$$

Finally, since by assumption $\lambda^+(x) \neq -\lambda^-(x) \quad$ for a.e $\quad x \in \sigma, \ \alpha = \beta = 0$ and the operator $\mathcal{H}^*$ is injective. □

In the next step, we provide some properties of the operator B. We need to introduce the operators $\mathcal{F} : \tilde{H}^{1/2}(\sigma) \times \tilde{H}^{-1/2}(\sigma) \to L^2(\mathbf{S}^{m-1})$ given by

$$\mathcal{F}(\varphi, \psi)(\hat{x}) := \gamma \int_\sigma \left(\varphi(y) \frac{\partial e^{-i\kappa \hat{x} y}}{\partial \nu(y)} + \psi(y) e^{-i\kappa \hat{x} y} \right) ds(y) \tag{28}$$

and $M : \tilde{H}^{1/2}(\sigma) \times \tilde{H}^{-1/2}(\sigma) \to H^{-1/2}(\sigma) \times H^{-1/2}(\sigma)$ defined by

$$M := \begin{pmatrix} T + \lambda^+(K + \frac{1}{2} I) & -\lambda^+ S - K' + \frac{1}{2} I \\ T - \lambda^-(K - \frac{1}{2} I) & \lambda^- S - K' - \frac{1}{2} I \end{pmatrix}. \tag{29}$$

Lemma 5 *The operator M has a bounded inverse and $B = \gamma \mathcal{F} M^{-1}$.*

Proof. For a given $(\varphi,\psi)\in \tilde{H}^{1/2}(\sigma)\times\tilde{H}^{-1/2}(\sigma)$, the function $\mathcal{F}(\varphi,\psi)(\hat{x})$ is the far field pattern of the potential

$$P(\varphi,\psi)(x):=\int_\sigma \varphi(y)\frac{\partial\Phi(x,y)}{\partial\nu(y)}ds(y)+\int_\sigma\psi(y)\Phi(x,y)ds(y).$$

The function $P\in H^1_{loc}(\mathbf{R}^m\setminus\bar{\sigma})$ satisfies the Helmholtz equation in $\mathbf{R}^m\setminus\bar{\sigma}$ and the Sommerfeld radiation condition. In addition, following the proof of Lemma 2, we show that $\varphi=[P]$, $\psi=-[\partial_\nu P]$ and

$$\begin{pmatrix}(\partial_\nu+\lambda^+)P^+(\varphi,\psi)\\(\partial_\nu-\lambda^-)P^-(\varphi,\psi)\end{pmatrix}=M\begin{pmatrix}\varphi\\\psi\end{pmatrix}$$

where $M:\tilde{H}^{1/2}(\sigma)\times\tilde{H}^{-1/2}(\sigma)\to H^{-1/2}(\sigma)\times H^{-1/2}(\sigma)$ is given by (29). This operator is related to the matrix A_σ defined by (7). More precisely,

$$A_\sigma=\begin{pmatrix}\lambda^-I & \lambda^+I\\ I & -I\end{pmatrix}M$$

and by Lemma 3, $M^{-1}:H^{-1/2}(\sigma)\times H^{-1/2}(\sigma)\to\tilde{H}^{1/2}(\sigma)\times\tilde{H}^{-1/2}(\sigma)$ exists and is bounded. □

Lemma 6 *The operator $\mathcal{F}:\tilde{H}^{1/2}(\sigma)\times\tilde{H}^{-1/2}(\sigma)\to L^2(\mathbf{S}^{m-1})$ is injective and has a dense range in $L^2(\mathbf{S}^{m-1})$.*

Proof. The injectivity of $\mathcal{F}$ can be proved in the same way as in Lemma 4, by replacing the potential V by P.
Proceeding again as in the proof of Lemma 4, let $g\in L^2(\mathbf{S}^{m-1})$ and $(\alpha,\beta)\in\tilde{H}^{1/2}(\sigma)\times\tilde{H}^{-1/2}(\sigma)$,

$$\begin{aligned}\langle\mathcal{F}(\alpha,\beta),g\rangle&=\int_{\mathbf{S}^{m-1}}g(d)\mathcal{F}(\alpha,\beta)(d)ds(d)\\&=\gamma\int_{\mathbf{S}^{m-1}}g(d)\left(\int_\sigma\alpha(y)\frac{\partial e^{-i\kappa d\cdot y}}{\partial\nu(y)}ds(y)+\int_\sigma\beta(y)e^{-i\kappa d\cdot y}ds(y)\right)ds(d)\\&=\gamma\int_\sigma\alpha(y)\int_{\mathbf{S}^{m-1}}g(d)\frac{\partial e^{-i\kappa d\cdot y}}{\partial\nu(y)}ds(d)ds(y)+\gamma\int_\sigma\beta(y)\int_{\mathbf{S}^{m-1}}g(d)e^{-i\kappa d\cdot y}ds(d)ds(y).\end{aligned}$$

Therefore, $\mathcal{F}^*(g)=\gamma(\partial_\nu v_g,v_g)$.
Now, if $\mathcal{F}^*(g)=0$ then $v_g=\partial_\nu v_g=0$.
Thus, as in Lemma 4, $g=0$ which proves the density of the range of $\mathcal{F}$. □

Summarizing the previous results, the operator F defined by (22) is factorized as $F=\mathcal{F}M^{-1}\mathcal{H}$. Hence, the range of F is included in the range of $\mathcal{F}$. Therefore, thanks to the following Lemma, there exist an approximated solution of the equation (23).

Lemma 7 *For any smooth non intersecting arc L and functions $\alpha_L\in\tilde{H}^{\frac{1}{2}}(L)$, $\beta_L\in\tilde{H}^{-\frac{1}{2}}(L)$, the operator Φ_L^∞ given by (24) belongs to $R(\mathcal{F})$ the range of $\mathcal{F}$ if and only $L\subset\sigma$.*

Proof.
First assume that $L\subset\sigma$. Since $\tilde{H}^{\pm\frac{1}{2}}(L)\subset\tilde{H}^{\pm\frac{1}{2}}(\sigma)$, it follows from (28) that $\Phi_L^\infty(\hat{x})\in R(\mathcal{F})$.

Now let $L\not\subset\sigma$ and assume, on the contrary, that $\Phi_L^\infty\in R(\mathcal{F})$. Hence, there exists $\varphi\in\tilde{H}^{\frac{1}{2}}(\sigma)$ and $\psi\in\tilde{H}^{-\frac{1}{2}}(\sigma)$ such that

$$\Phi_L^\infty(\hat{x})=\gamma\int_L\left(\varphi(y)\frac{\partial e^{-i\kappa\hat{x}\cdot y}}{\partial\nu(y)}+\psi(y)e^{-i\kappa\hat{x}\cdot y}(y)\right)ds(y).$$

Thus Φ_L^∞ is the far field pattern of the potential

$$P(x)=\int_\sigma\left(\varphi(y)\frac{\partial\Phi(x,y)}{\partial\nu(y)}+\psi(y)\Phi(x,y)\right)ds(y),\quad x\in R^{m-1}\setminus\overline{\sigma}.$$

Since by definition Φ_L^∞ is also the far field pattern of the potential Φ_L given by (26) then using the Rellich lemma and the unique continuation principle, the potentials Φ_L and P coincide in $R^{m-1} \setminus (\bar{\sigma} \cup \bar{L})$.
Let $x_0 \in L \backslash \overline{\sigma}$ and B_ϵ a small neighborhood of x_0 with $B_\epsilon \cap \sigma = \emptyset$. Then, P is analytic in B_ϵ while Φ_L has a singularity at x_0 which is a contradiction. This proves that $\Phi_L^\infty \notin R(\mathcal{F})$. □

Theorem 3 *We assume that L is a nonintersecting smooth open arc. The following is true:*

1. *If $L \subset \sigma$; there exists a sequence $(g_n)_{n\in\mathbb{N}}$ on $L^2(S^{m-1})$ such that*

$$\lim_{n\to+\infty} \|F(g_n) - \Phi_L^\infty\|_{L^2(S^{m-1})} = 0$$

and

$$\lim_{n\to+\infty} ||v_{g_n}||_* < \infty,$$

where $\|v_{g_n}\|_* := \|\partial_\nu v_{g_n} + \lambda^+ v_{g_n}\|_{H^{-\frac{1}{2}}(\sigma)} + \|\partial_\nu v_{g_n} - \lambda^- v_{g_n}\|_{H^{-\frac{1}{2}}(\sigma)}$.

2. *Otherwise, for any sequence $(g_n)_{n\in\mathbb{N}} \subset L^2(S^{n-1})$ that satisfies*

$$\lim_{n\to+\infty} \|F(g_n) - \Phi_L^\infty\|_{L^2(S^{m-1})} = 0$$

we have

$$\lim_{n\to+\infty} ||v_{g_n}||_* = +\infty.$$

Proof.

- If $L \subset \sigma$, it is easy to find a bounded solution of the far field equation (23). In fact, we have $\tilde{H}^{\frac{1}{2}}(L) \subset \tilde{H}^{\frac{1}{2}}(\sigma)$ and $\tilde{H}^{-\frac{1}{2}}(L) \subset \tilde{H}^{-\frac{1}{2}}(\sigma)$.
  Thus, $\Phi_L^\infty \in R(\mathcal{F})$ there exists a unique $(\alpha, \beta) \in \tilde{H}^{\frac{1}{2}}(\sigma) \times \tilde{H}^{-\frac{1}{2}}(\sigma)$ such that

$$\Phi_L^\infty = \mathcal{F}(\alpha, \beta)$$

  Therefore by Lemma 5 there exists a unique $(\tilde{\alpha}, \tilde{\beta}) \in \tilde{H}^{\frac{1}{2}}(\sigma) \times \tilde{H}^{-\frac{1}{2}}(\sigma)$ such that

$$\Phi_L^\infty = \mathcal{F}M^{-1}(\tilde{\alpha}, \tilde{\beta})^T.$$

  Moreover by Lemma 4 the range of $\mathcal{H}$ is dense on $H^{-1/2}(\sigma) \times H^{-1/2}(\sigma)$, hence there exists $(\alpha_n, \beta_n)_{n\in\mathbb{N}} \subset R(\mathcal{H})$ such that $\lim_{n\to+\infty}(\alpha_n, \beta_n) = (\tilde{\alpha}, \tilde{\beta})$. Using the continuity of $\mathcal{H}$, we show the existence of a sequence $(g_n)_{n\in\mathbb{N}} \subset L^2(S^{n-1})$ verifying $\lim_{n\to\infty} \mathcal{H}g_n = (\tilde{\alpha}, \tilde{\beta})$ which proves that

$$\lim_{n\to+\infty} \|F(g_n) - \Phi_L^\infty\|_{L^2(S^{m-1})} = 0.$$

- Let $L \not\subset \sigma$ and let us assume that $\|v_{g_n}\|_* < \infty$. Therefore,

$$\|\partial_\nu v_{g_n} + \lambda^+ v_{g_n}\|_{H^{-\frac{1}{2}}(\sigma)} + \|\partial_\nu v_{g_n} - \lambda^- v_{g_n}\|_{H^{-\frac{1}{2}}(\sigma)} < \infty. \tag{30}$$

  Let $(\alpha_n, \beta_n) \in R(\mathcal{H})$. Since $\mathcal{H}$ is injective there exists a sequence $(g_n)_{n\in\mathbb{N}} \subset L^2(S^{n-1})$ such that $\mathcal{H}(g_n) = (\alpha_n, \beta_n)$. From (30), the sequence (α_n, β_n) is bounded in $H^{-\frac{1}{2}}(\sigma) \times H^{-\frac{1}{2}}(\sigma)$. Therefore we can extract a subsequence, that we still denote (α_n, β_n) which weakly converges to (α, β).
  The integral operator $\mathcal{F}$ is compact since it has a regular kernal and M^{-1} is a bounded operator, so that the operator $\mathcal{F}M^{-1}$ is a compact operator. Consequently,

$$\lim_{n\to+\infty} \|F(g_n) - \mathcal{F}M^{-1}(\alpha, \beta)\|_{L^2(S^{m-1})} = 0$$

  and by the uniqueness of the limit, we have

$$\mathcal{F}M^{-1}(\alpha, \beta) = \Phi_L^\infty.$$

  We deduce that $\Phi_L^\infty \in R(\mathcal{F})$ and $L \subset \sigma$ which is a contradiction. □

3.2 Numerical schemes and results

Regularization

For the purpose of the numerical experiments, we construct a nearby solution to (23) using a Tikhonov regularization. Therefore we solve the following equation

$$(\eta I + F^*F)g_\eta = F^*\Phi_L^\infty$$

where η is a parameter of regularization. By the singular value decomposition (SVD) we mean a representation of F in the form

$$F(g) = \sum_i \sigma_i(g, f_i)l_i,$$

where (f_i), (l_i) are orthonormal systems in $L^2(S^1)$, and σ_i are positive constants, the singular values of F. The adjoint of F is given by

$$F^*(g) = \sum_i \sigma_i(g, l_i)f_i,$$

Thus, the operator F^*F is given by

$$F^*F(g) = \sum_i \sigma_i^2(g, f_i)f_i,$$

On the other hand, we have

$$F^*(\Phi_L^\infty) = \sum_i \sigma_i(\Phi_L^\infty, l_i)f_i.$$

Finally, we get the expression of g_η, the solution of (23)as

$$g_\eta = \sum_i \frac{\sigma_i(\Phi_L^\infty, l_i)}{\eta + \sigma_i^2} f_i \tag{31}$$

The regularization parameter is chosen using the Morozov discrepancy principle.

Discretization

The numerical experiments are conducted in a 2 D setting of the problem. We consider n equally distant observation points of the far field $(\hat{x}_l)_{1\leq l\leq n}$ on the unit circle.

$$Fg(\hat{x}_l) \simeq \sum_{j=1}^{n} w_j u_\infty(\hat{x}_l, \hat{x}_j)g(\hat{x}_j) \tag{32}$$

where w_j is the arclengh between two adjacent points. Let L be a small segment of center z and with normal ν. Then

$$\Phi_L^\infty(\hat{x}_l) \simeq \gamma|L|(\alpha(z)e^{-ik\hat{x}_l z} + \beta(z)(-ik\hat{x}_l.\nu)e^{-ik\hat{x}_l z}) \tag{33}$$

The discrete equation to solve is then

$$Fg(\hat{x}_l) \simeq \Phi_L^\infty(\hat{x}_l) \qquad \forall \hat{x}_l \tag{34}$$

using the Tikhonov procedure explained above. The sampling procedure will consist then in varying the z and ν in (33). According to Theorem 3 we expect $\|g\|$ (where g is a solution to (34)) to be large except when $z \in \sigma$ and ν is the normal to σ at z.
We shall consider two types of solutions: the first one denoted by g_z corresponds to $\alpha(z) = 1$ and $\beta(z) = 0$, the second one denoted by $g_{z,\nu}$ corresponds to $\alpha(z) = 0$ and $\beta(z) = 1$.

First criterion
Let us consider two independent normals for instance $\nu_1 = (0,1)^t$ and $\nu_2 = (1,0)^t$. At each sampling point z we compute

$$z \quad \longrightarrow \quad \frac{1}{\|g_z\|} + \frac{1}{\|g_{z,\nu_1}\|} + \frac{1}{\|g_{z,\nu_2}\|}. \tag{35}$$

This criterion may not be efficient if ν_1 or ν_2 coincide with the exact normal to σ at z, specially if σ is a segment with normal N, $N \neq \nu_1$ and $N \neq \nu_2$ (see numerical section).

Second criterion
Let us define the normal ν as follows:

$$\nu = \zeta\nu_1 + \sqrt{1-\zeta^2}\nu_2 \qquad \text{with } 0 \leq \zeta \leq 1$$

Therefore, by linearity of the equation (34)

$$g_{z,\nu} = \zeta g_{z,\nu_1} + \sqrt{1-\zeta^2} g_{z,\nu_2}.$$

Based on the theoretical justification, the normal ν to σ at $z \in \sigma$ corresponds with the value ζ that minimizes

$$\|g_{z,\nu}\|^2 = \zeta^2\|g_{z,\nu_1}\|^2 + (1-\zeta^2)\|g_{z,\nu_2}\|^2 + 2\zeta(1-\zeta^2)\,\langle g_{z,\nu_1}\ , g_{z,\nu_2}\rangle \tag{36}$$

The proposed criterion will be the determination on each point z of

$$z \quad \longrightarrow \quad \frac{1}{\|g_z\|} + \frac{1}{\|g_{z,\nu}\|} \tag{37}$$

where g, $g_{z,\nu}$ corresponds with ζ that minimizes (36).

Numerical tests

The efficiency of this approach is tested using both criteria for different shapes, namely arc-shaped cracks, L-shaped cracks and the union of two segments having an oblique angle between them and for several ranges of the impedance values. We present in the following figures the isovalues of the right hand side of (35). The red isovalues correspond to the highest values whereas the blue ones represent the smallest ones. This means that the crack corresponds to red isovalues in the figures.
In all the numerical tests we use 100 observation points of the far field pattern and the same number of incident plane waves.
Both criteria give a good reconstruction of the crack for the case of large impedances (see Figures 7, 8). In the case of small impedances, using the first criterion, the result is not satisfactory for all geometries. This is due to the fact that for large impedances we are close to the Dirichlet case, hence the dominant term in (35) is $\frac{1}{\|g_z\|}$. In the case of the small impedances, we are close to the Neumann case and in this case the dominant term is the one that contains the normal derivatives. Figure 9 shows that if ν_1 or ν_2 coincides with the exact normal to the crack we have a good reconstruction otherwise only the part of the crack for which the normal coincides with ν_1 or ν_2 is correctly reconstructed: see Figure 10, 11. Hence having a good approximation of ν is very important for the precision of the result. This problem is fixed by the use of the second criterion as demonstrated by the reconstruction shown in Figures 7, 8, 9, 10 and 11. Let us observe however that the quality of the results slightly deteriorates when the impedance values are between high and small magnitudes: see Figure 12, 13 and 14. To illustrate the importance of the reconstruction of the normals in the precision of the results we visualize the reconstructed ones in Figure 15, 16 and 17. We observe that the best results correspond with the cases where the normals at the crack are the exact ones.

Case of Large impedances

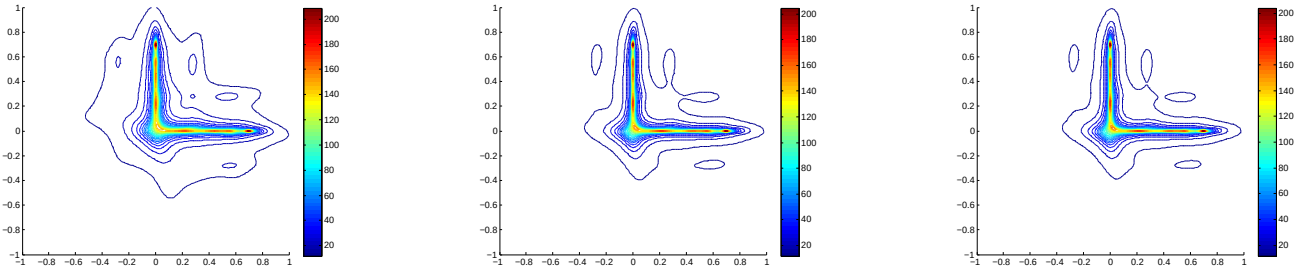

(a) Reconstruction using the first criterion

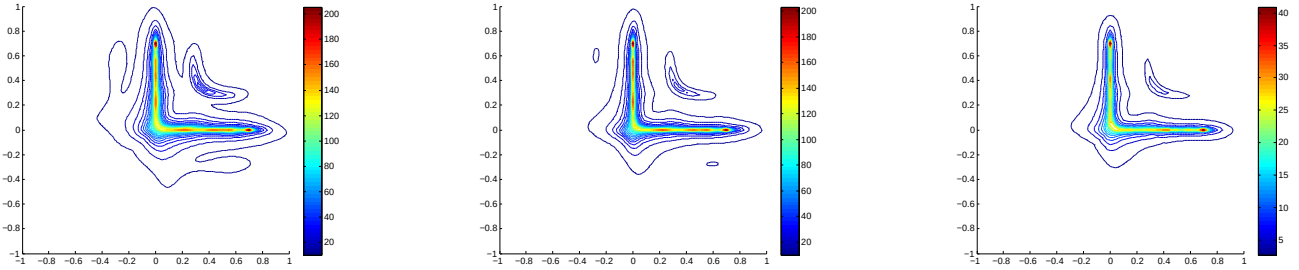

(b) Reconstruction using the second criterion

Figure 7: Reconstruction of an L-shaped crack with peaks $(0.75, 0), (0, 0), (0, 0.75)$ for $\lambda^- = \lambda^+ = 100(1 + i)$ (left), $\lambda^- = \lambda^+ = 1000(1 + i)$ (middle), $\lambda^- = \lambda^+ = 10^6(1 + i)$ (right)

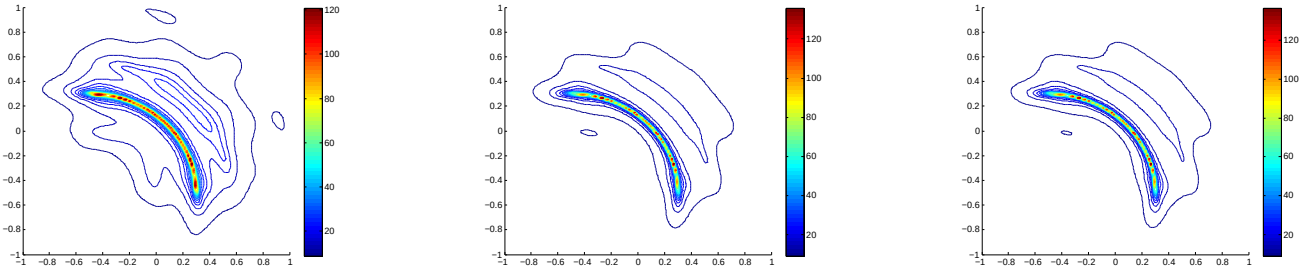

(a) Reconstruction using the first criterion

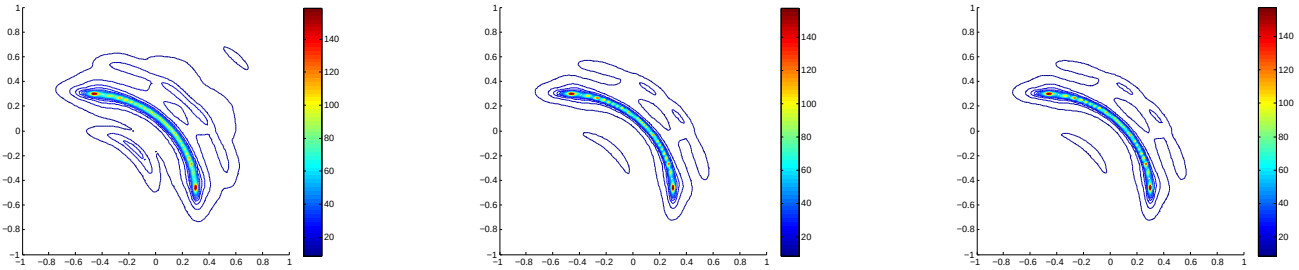

(b) Reconstruction using the second criterion

Figure 8: Reconstruction of an arc-shaped crack with center $(-0.5, -0.5)$, radius 0.8 and angle varying from 0 to 90 degrees for $\lambda^- = \lambda^+ = 100(1 + i)$ (left), $\lambda^- = \lambda^+ = 1000(1 + i)$ (middle), $\lambda^- = \lambda^+ = 10^6(1 + i)$ (right).

Case of small impedances

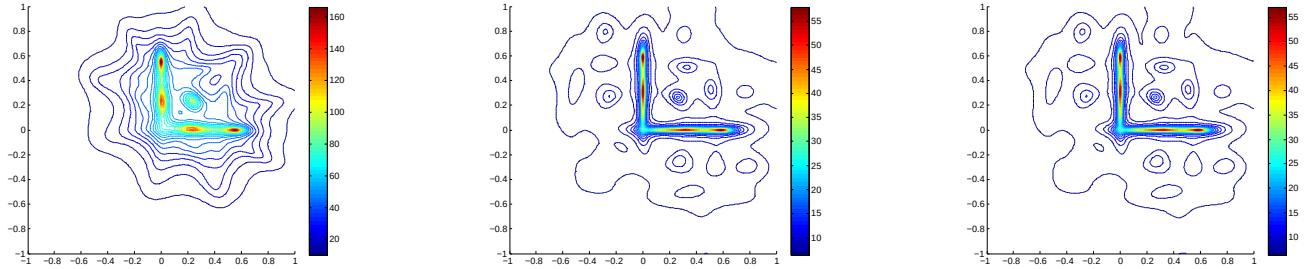

(a) Reconstruction using the first criterion

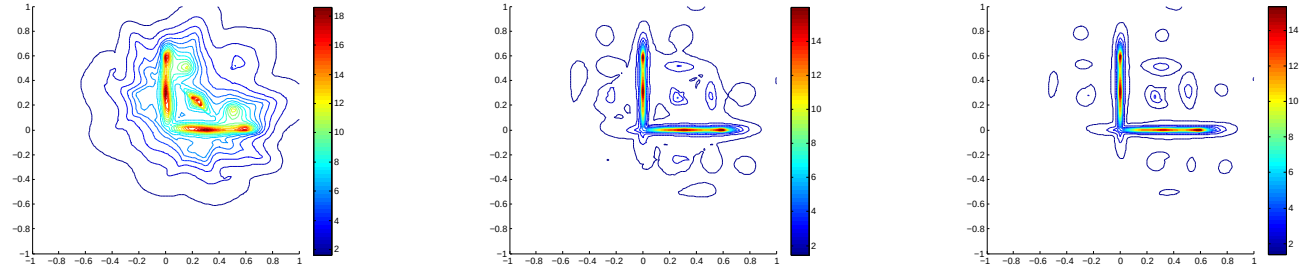

(b) Reconstruction using the second criterion

Figure 9: Reconstruction of an L-shaped crack with peaks $(0, 0.75), (0, 0), (0.75, 0)$ for $\lambda^- = \lambda^+ = 0.1(1+i)$ (left), $\lambda^- = \lambda^+ = 0.01(1+i)$ (middle) $\lambda^- = \lambda^+ = 10^{-6}(1+i)$ (right).

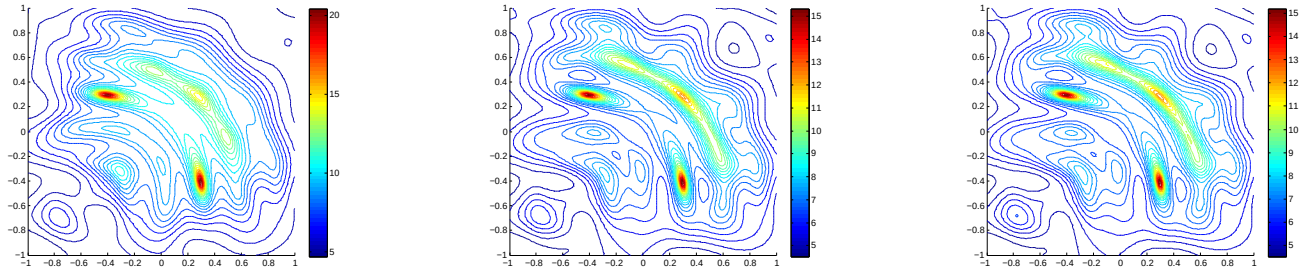

(a) Reconstruction using the first criterion

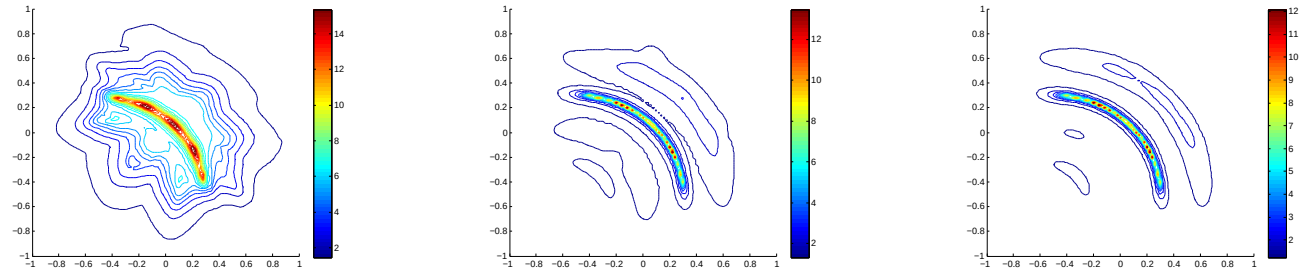

(b) Reconstruction using the second criterion

Figure 10: Reconstruction of an arc-shaped crack with center $(-0.5, -0.5)$, radius 0.8 and angle varying from 0 to 90 degrees for $\lambda^- = \lambda^+ = 0.1(-1+i)$ (left), $\lambda^- = \lambda^+ = 0.01(-1+i)$ (middle), $\lambda^- = \lambda^+ = 10^{-6}(-1+i)$ (right).

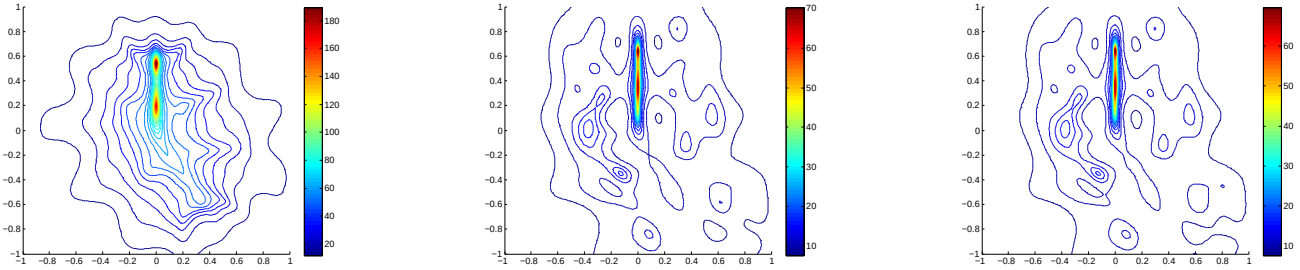

(a) Reconstruction using the first criterion

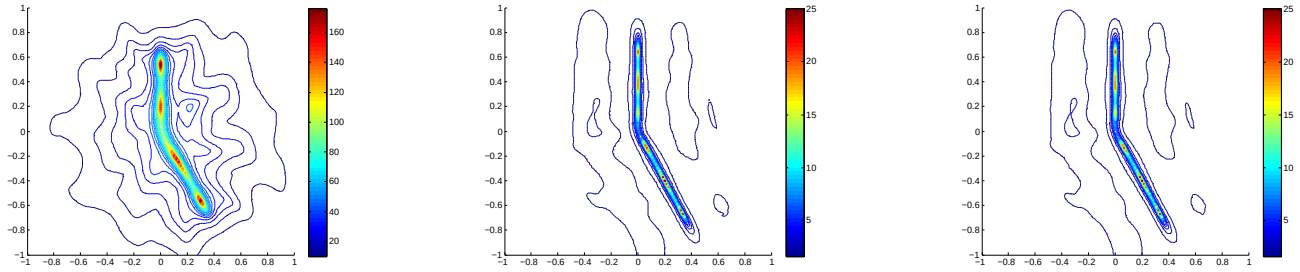

(b) Reconstruction using the second criterion

Figure 11: Reconstruction of two segments $\{0\} \times [0, 0.8]$ and $[0, 0.4] \times [0, -0.8]$ for $\lambda^- = \lambda^+ = 0.1(1+i)$ (left), $\lambda^- = \lambda^+ = 0.01(1+i)$ (middle), $\lambda^- = \lambda^+ = 10^{-6}(1+i)$ (right).

Case of impedances with "moderate values"

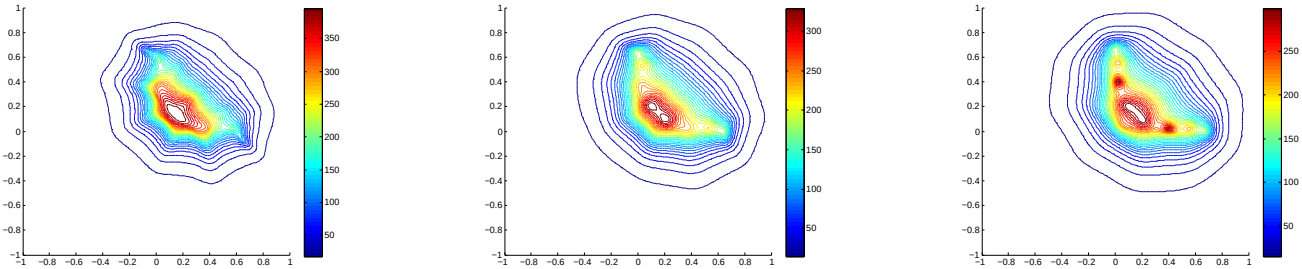

(a) Reconstruction using the first criterion

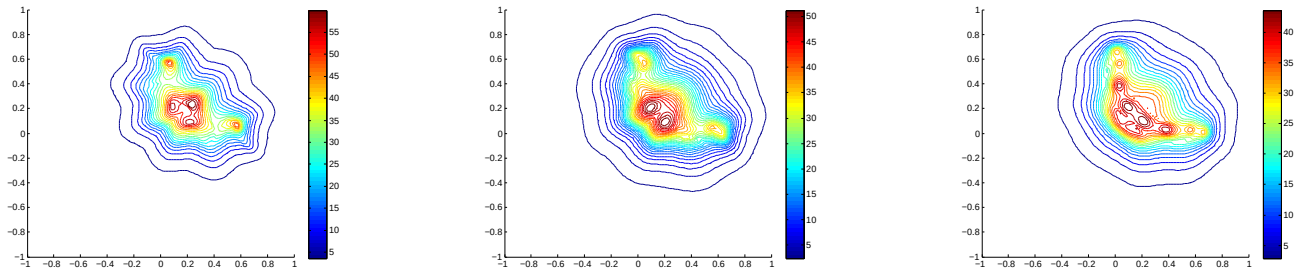

(b) Reconstruction using the second criterion

Figure 12: Reconstruction of an L-shaped crack with peaks $(0, 0.75), (0, 0), (0.75, 0)$ for $\lambda^- = 1.5+1$ and $\lambda^+ = 2 + 1.2i$ (left), $\lambda^- = \lambda^+ = 5(1+i)$ (middle), $\lambda^- = \lambda^+ = 10(1+i)$ (right).

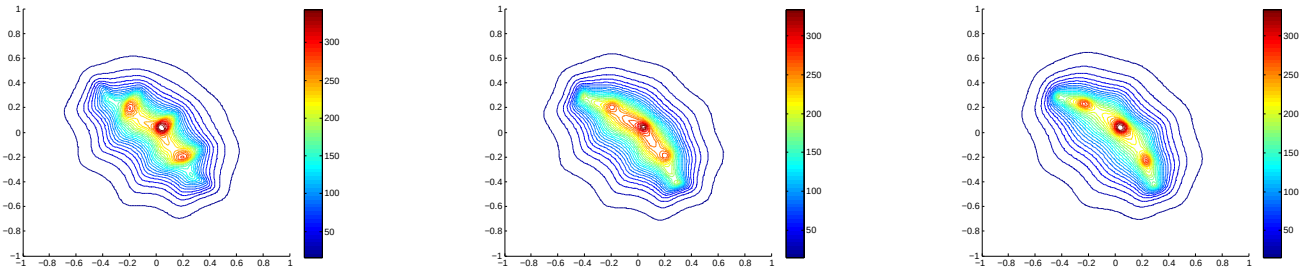

(a) Reconstruction using the first criterion

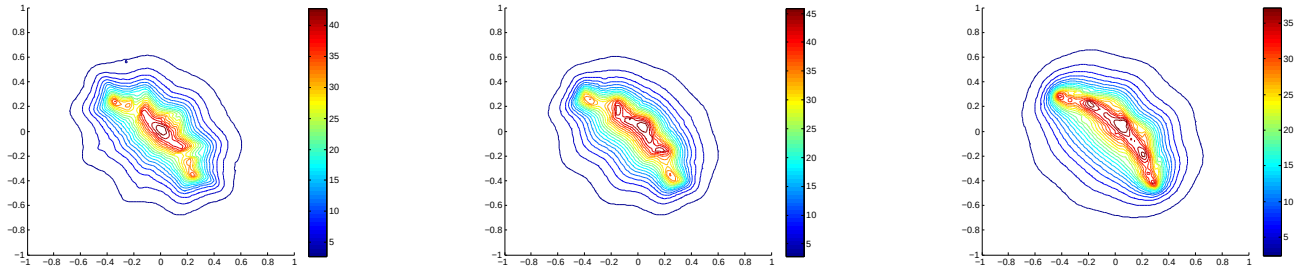

(b) Reconstruction using the second criterion

Figure 13: Reconstruction of an arc-shaped crack with center $(-0.5, -0.5)$, radius 0.8 and angle varying from 0 to 90 degrees for $\lambda^- = 1.5 + i$ and $\lambda^+ = 2 + 1.2i$ (left), $\lambda^- = \lambda^+ = 5 + 5i$ (middle), $\lambda^- = \lambda^+ = 10(1 + i)$ (right).

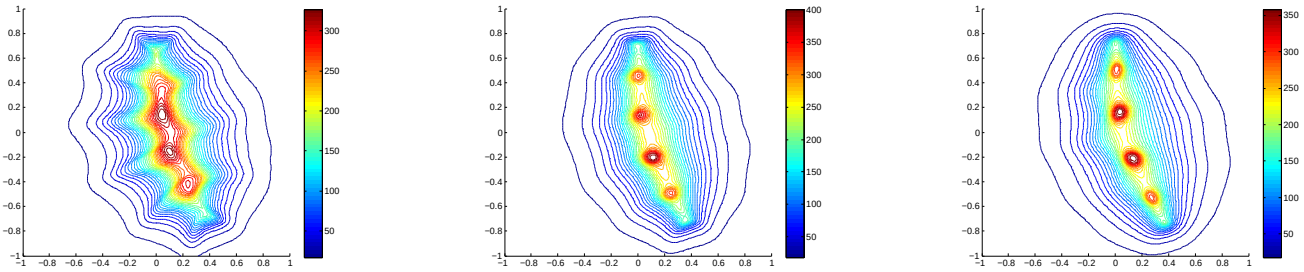

(a) Reconstruction using the first criterion

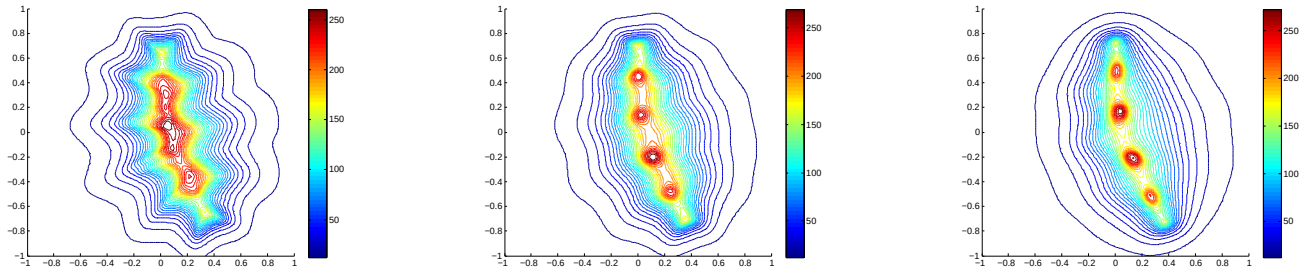

(b) Reconstruction using the second criterion

Figure 14: Reconstruction of two segments $\{0\} \times [0, 0.8]$ and $[0, 0.4] \times [0, -0.8]$ for $\lambda^- = 1.5 + i$ and $\lambda^+ = 2 + 1.2i$ (left), $\lambda^- = \lambda^+ = 5 + 5i$ (middle), $\lambda^- = \lambda^+ = 10(1 + i)$ (right).

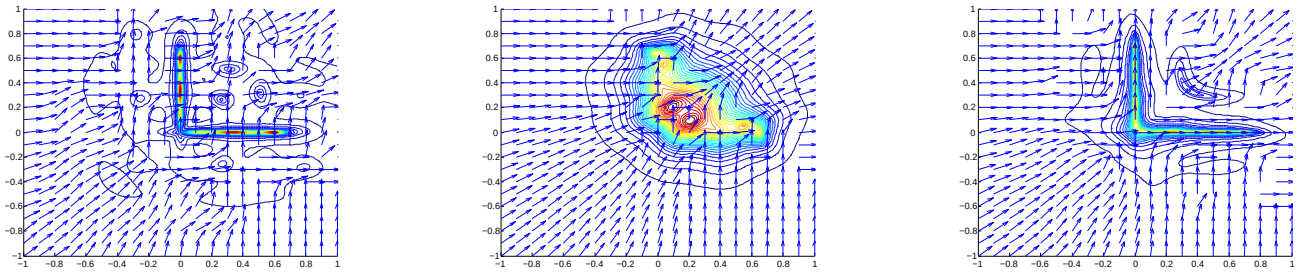

Figure 15: Reconstruction of the normals for $\lambda^- = \lambda^+ = 0.001 + 0.001i$ (left), $\lambda^- = \lambda^+ = 5 + 5i$ (middle), $\lambda^- = \lambda^+ = 10(1 + i)$ (right).

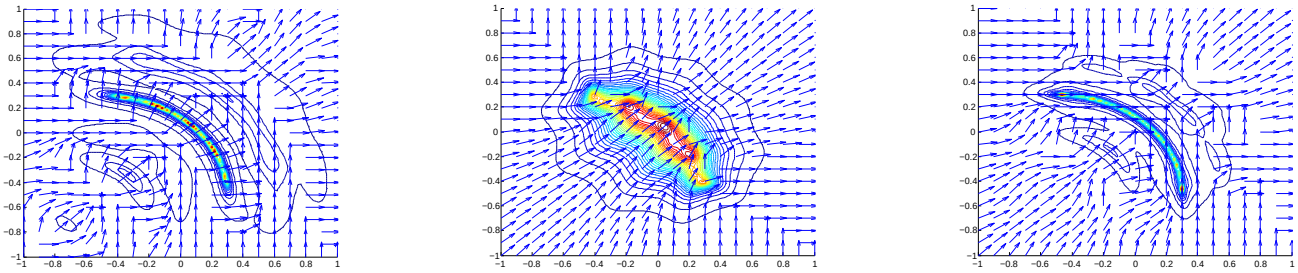

Figure 16: Reconstruction of the normals for $\lambda^- = \lambda^+ = 0.001 + 0.001i$ (left), $\lambda^- = \lambda^+ = 5 + 5i$ (middle), $\lambda^- = \lambda^+ = 10(1 + i)$ (right).

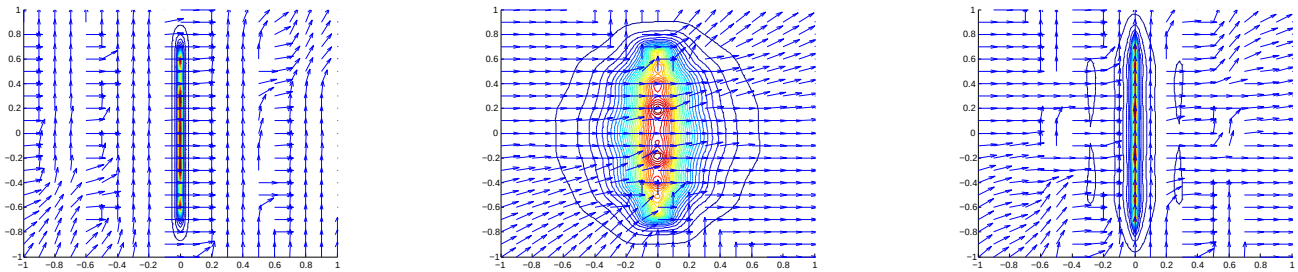

Figure 17: Reconstruction of the normals for $\lambda^- = \lambda^+ = 0.001 + 0.001i$ (left), $\lambda^- = \lambda^+ = 5 + 5i$ (middle), $\lambda^- = \lambda^+ = 10(1 + i)$ (right).

Influence of the frequency

A more relevant physical model for the impedance boundary conditions would be

$$\partial_\nu u^\pm \pm k\tilde{\lambda}^\pm u^\pm = 0 \qquad \text{on} \quad \sigma^\pm$$

where now $\lambda^\pm$ are dimensionless constants. We shall study the influence of the frequency on the reconstructions for these type of conditions. Figures 18, 19 show the reconstructions of the normals for two different choices of the frequency. We observe that the best orientation for the normals are given by the smaller frequency. This then suggests to use the small frequency case to first reconstruct the normal fields then use these normals to evaluate the criterion (37). This procedure

improves the results obtained for the higher frequency: compare Figures 20-22 to Figures 12-14 respectively.

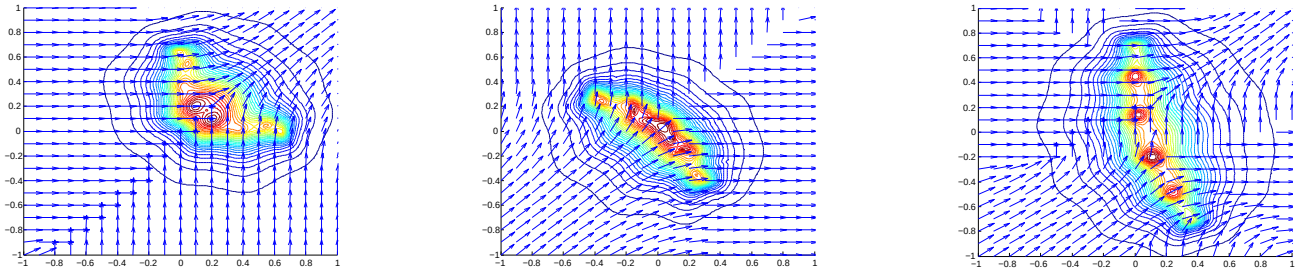

Figure 18: Reconstruction of the normals for $\tilde{\lambda}^- = \tilde{\lambda}^+ = 0.79(1+i)$, $k = \pi/2$.

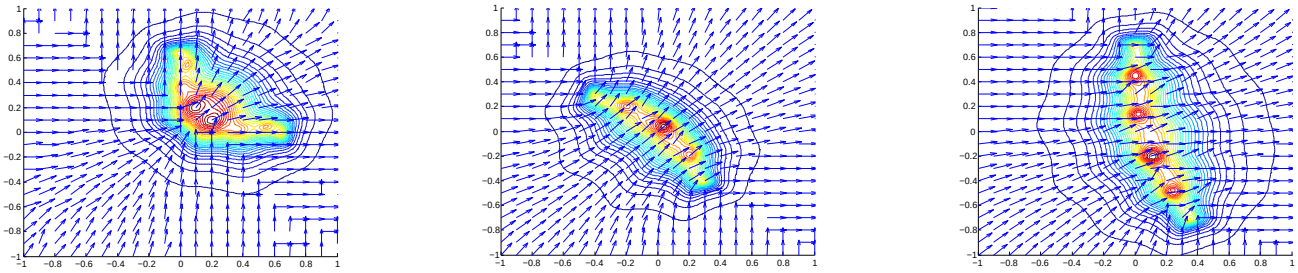

Figure 19: Reconstruction of the normals for $\tilde{\lambda}^- = \tilde{\lambda}^+ = 0.79(1+i)$, $k = 4\pi$.

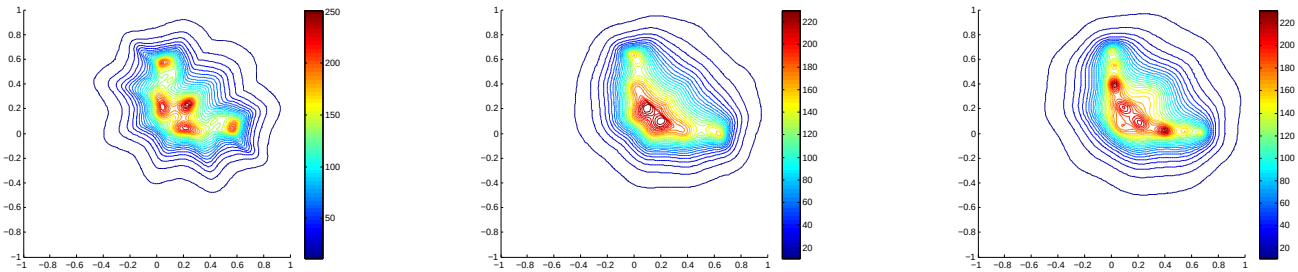

Figure 20: Reconstruction of an L-shaped crack with peaks $(0, 0.75), (0, 0), (0.75, 0)$ for $\tilde{\lambda}^+ = 0.23 + 0.15i \quad \tilde{\lambda}^- = 0.31 + 0.19i$ (left) $\tilde{\lambda}^- = \tilde{\lambda}^+ = 0.79(1+i)$ (middle) $\tilde{\lambda}^- = \tilde{\lambda}^+ = 1.58(1+i)$ (right) with $k = 2\pi$.

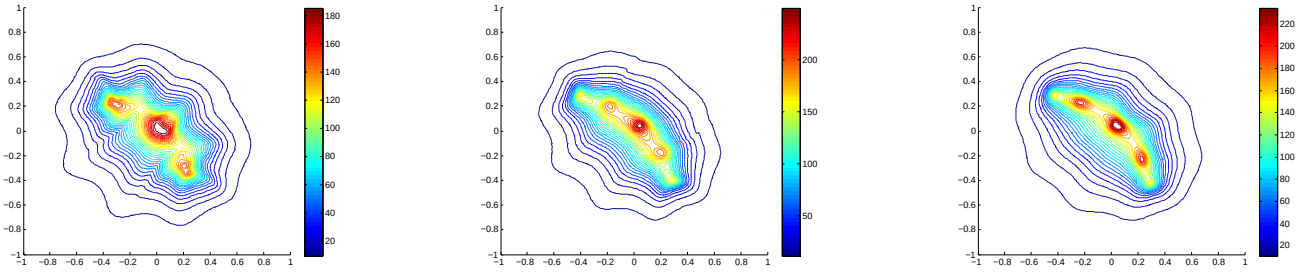

Figure 21: Reconstruction of arc-shaped crack for $\tilde{\lambda}^+ = 0.23 + 0.15i \quad \tilde{\lambda}^- = 0.31 + 0.19i$ (left) $\tilde{\lambda}^- = \tilde{\lambda}^+ = 0.79(1+i)$ (middle) $\tilde{\lambda}^- = \tilde{\lambda}^+ = 1.58(1+i)$ (right) with $k = 2\pi$.

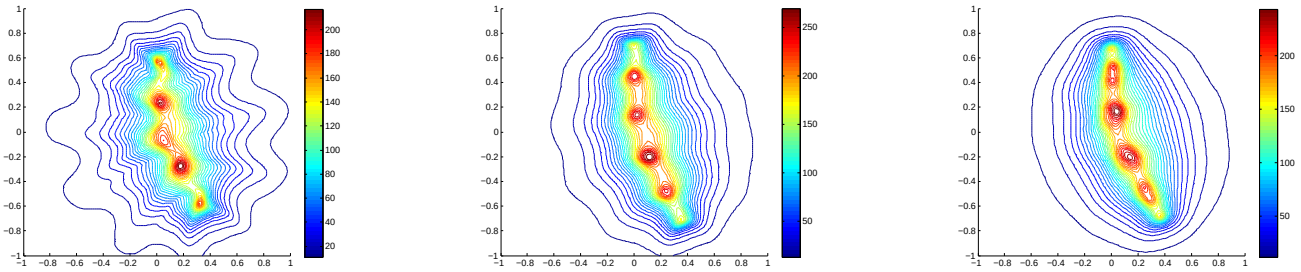

Figure 22: Reconstruction of two segments $\{0\} \times [0, 0.8]$ and $[0, 0.4] \times [0, -0.8]$ for $\tilde{\lambda}^+ = 0.23 + 0.15i \quad \tilde{\lambda}^- = 0.31 + 0.19i$ (left) $\tilde{\lambda}^- = \tilde{\lambda}^+ = 0.79(1+i)$ (middle) $\tilde{\lambda}^- = \tilde{\lambda}^+ = 1.58(1+i)$ (right) with $k = 2\pi$.

References

[1] F. Cakoni and D. Colton. The linear sampling method for cracks. *Inverse Problems*, 19:279–295, 2003.

[2] D. Colton and H. Haddar. An application of the reciprocity gap functionnal to inverse scattering theory. *Inverse Problems*, 21:383–398, 2005.

[3] D. Colton and R. Kress. *Inverse acoustic and electromagnetic scattering theory, second ed.* Springer-Verlag, 1998.

[4] F. Delbary. *Identifications de fissures par des ondes acoustiques.* PhD thesis, Université de Paris 6, 2006.

[5] M. A. Hamdi. *Formulation variationnelle par équations intégrales pour le calcul de champs acoustiques linéaire proches et lointains.* PhD thesis, Université de Technologie de Compiègne, 1982.

[6] F. Hecht. *FreeFem++, Third edition, version 3.10-2.* Laboratoire Jacques-Louis Lions, Université Pierre et Marie Curie, Paris, 2010.

[7] A. Kirsh and N. Grinberg. *The Factorization method for inverse problem.* Oxford lecture series in Mathematics and its applications, 2008.

[8] A. Kirsh and S. Ritter. A linear sampling method for inverse scattering from an open arc. *inverse Problems*, 16:89–105, 2000.

[9] R. Kress and K.-M. Lee. Integral equation methods for scattering from an impedance crack. *J. Comput. Appl. Math.*, 161:161–177, 2003.

[10] J. Liu and M. Sini. Reconstruction of cracks of different types from far-field measurements. *Math. Meth. Appl. Sci*, 33:950–973, 2010.

[11] W. McLean. *Strongly Elliptic Systems and Boundary Integral Equations*. Cambridge University Press, Cambridge, 2000.

Centre de recherche INRIA Saclay – Île-de-France
Parc Orsay Université - ZAC des Vignes
4, rue Jacques Monod - 91893 Orsay Cedex (France)

Centre de recherche INRIA Bordeaux – Sud Ouest : Domaine Universitaire - 351, cours de la Libération - 33405 Talence Cedex
Centre de recherche INRIA Grenoble – Rhône-Alpes : 655, avenue de l'Europe - 38334 Montbonnot Saint-Ismier
Centre de recherche INRIA Lille – Nord Europe : Parc Scientifique de la Haute Borne - 40, avenue Halley - 59650 Villeneuve d'Ascq
Centre de recherche INRIA Nancy – Grand Est : LORIA, Technopôle de Nancy-Brabois - Campus scientifique
615, rue du Jardin Botanique - BP 101 - 54602 Villers-lès-Nancy Cedex
Centre de recherche INRIA Paris – Rocquencourt : Domaine de Voluceau - Rocquencourt - BP 105 - 78153 Le Chesnay Cedex
Centre de recherche INRIA Rennes – Bretagne Atlantique : IRISA, Campus universitaire de Beaulieu - 35042 Rennes Cedex
Centre de recherche INRIA Sophia Antipolis – Méditerranée : 2004, route des Lucioles - BP 93 - 06902 Sophia Antipolis Cedex

Éditeur
INRIA - Domaine de Voluceau - Rocquencourt, BP 105 - 78153 Le Chesnay Cedex (France)
http://www.inria.fr
ISSN 0249-6399